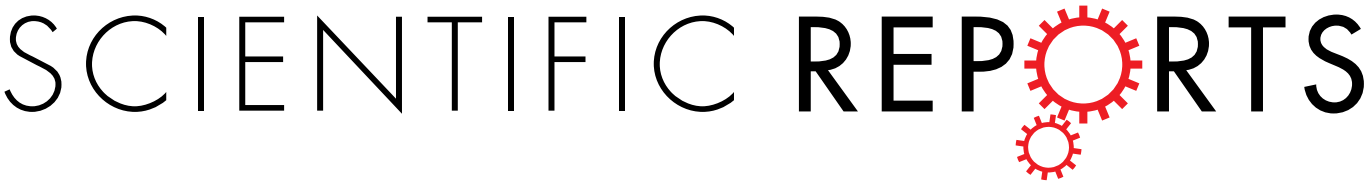

OPEN

Received: 18 February 2016
Accepted: 17 May 2016
Published: 06 June 2016

Smart window coating based on F-TiO_2-K_xWO_3 nanocomposites with heat shielding, ultraviolet isolating, hydrophilic and photocatalytic performance

Tongyao Liu[1], Bin Liu[1], Jing Wang[1], Linfen Yang[1], Xinlong Ma[1], Hao Li[1], Yihong Zhang[1], Shu Yin[2], Tsugio Sato[2], Tohru Sekino[3] & Yuhua Wang[1]

A series of smart window coated multifunctional NIR shielding-photocatalytic films were fabricated successfully through K_xWO_3 and F-TiO_2 in a low-cost and environmentally friendly process. Based on the synergistic effect of K_xWO_3 and F-TiO_2, the optimal proportion of K_xWO_3 to F-TiO_2 was investigated and the FT/2KWO nanocomposite film exhibited strong near-infrared, ultraviolet light shielding ability, good visible light transmittance, high photocatalytic activity and excellent hydrophilic capacity. This film exhibited better thermal insulation capacity than ITO and higher photocatalytic activity than P25. Meanwhile, the excellent stability of this film was examined by the cycle photocatalytic degradation and thermal insulation experiments. Overall, this work is expected to provide a possibility in integrating K_xWO_3 with F-TiO_2, so as to obtain a multifunctional NIR shielding-photocatalytic nanocomposite film in helping solve the energy crisis and deteriorating environmental issues.

Today, energy crisis and deteriorating environmental issues are posing serious threats to the sustainable development of human society. Thus, an increasing number of researches have focused on utilizing green techniques to deal with these aforementioned concerns in the past years[1–5]. As a critical component of buildings, windows can lose energy easily. Therefore, energy-efficient window coatings are considered to be the important step for reducing heat transfer between the indoor and outside environments. As a novel near-infrared (NIR) shielding material, the tungsten bronze (M_xWO_3), which is WO_3 doped with monovalent ions such as K^+, Na, NH_4^+ and others, has attracted great attention in recent years[6,7]. Compared with some transparent thermal insulation coatings like noble metals (Ag, Au)[8], black compounds (ruthenium dioxides, rhenium trioxides)[9], rare-earth hexaborides (lanthanum hexaborides)[10,11], and semiconductor oxides (ITO, ATO, AZO, etc.)[12–14], the NIR shielding ability and visible (Vis) transmittance of tungsten oxides can be remarkably superior due to the high free electron density, which can be utilized to produce localized surface plasma resonance[11,15]. Lately, our group have reported that cesium tungsten oxides (Cs_xWO_3) powders could be prepared by a water controlled-release solvothermal process with CsOH and WCl_6 as raw materials, and it could exhibit excellent visible transparency and broad waveband absorption of 800 to 15,000 nm[16,17]. However, these raw materials are not environmentally friendly because of the easy hydrolysis of WCl_6 and the volatilization of HCl[18]. To overcome this drawback, the one-dimensional potassium-doped tungsten bronze (K_xWO_3) powders were successfully synthesized with K_2WO_4 and K_2SO_4 through the hydrothermal process. The products could shield the NIR light with wavelength $\lambda > 1000$ nm, and this excellent heat shielding property implies that the K_xWO_3 might be the potential candidate for the smart window coated materials[19].

If a smart window coating could be developed to not only shield the NIR but also degrade harmful pollutants, it would have a huge impact on deteriorating environmental issues and present self-cleaning effect

[1]Department of Materials Science, School of Physical Science and Technology, Lanzhou University, Lanzhou, 730000, China. [2]Institute of Multidisciplinary Research for Advanced Materials, Tohoku University, 2-1-1 Katahira, Aoba-ku, Sendai, Japan. [3]The Institute of Scientific and Industrial Research, Osaka University, Japan. Correspondence and requests for materials should be addressed to B.L. (email: liubin@lzu.edu.cn) or Y.W. (email: wyh@lzu.edu.cn)

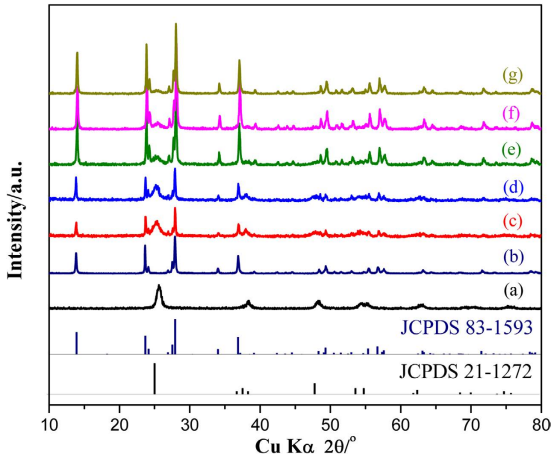

Figure 1. XRD patterns of pure (**a**) F-TiO_2, (**b**) K_xWO_3 and different FT-KWO nanocomposites: (**c**) 3FT/KWO, (**d**) 2FT/KWO, (**e**) FT/KWO, (**f**) FT/2KWO, (**g**) FT/3KWO.

simultaneously. Owing to photocatalytic and hydrophilic properties, semiconductor photocatalysts are widely and frequently employed to purify air and water contaminants[20,21]. Among various semiconductor photocatalysts, titanium dioxide (TiO_2) is the most suitable photocatalyst for widespread environmental applications because of its long-term stability against photocorrosion, excellent photocatalytic activity and strong absorption of harmful ultraviolet (UV) light[22–26]. Due to the fact that a photocatalytic reaction occurs at the interface between catalyst surfaces and organic pollutants, it is highly feasible that the photocatalytic activity of TiO_2 is strongly dependent on its surface properties[27,28]. Based on this speculation, surface-fluorinated TiO_2 (F-TiO_2) has been extensively investigated for its wonderful photocatalytic activity, which could be attributed to the enhanced generation of mobile free •OH radicals on the surface of F-TiO_2[29]. Thus, F-TiO_2 might be a promising photocatalyst to solve the environmental pollution concerns by relying on its highly efficient solar-light-driven photocatalytic activity[30].

In our recent research, Cs_xWO_3/ZnO nanocomposite was prepared as a smart coating for photocatalytic environmental cleanup and heat insulation[31]. Despite numerous advantages of this film, the less environmental friendliness of the preparation process and the instability of ZnO are in urgent need to be solved[32,33]. In this work, a series of multifunctional NIR shielding-photocatalytic nanocomposite films were fabricated successfully through F-TiO_2 and K_xWO_3. In these smart coatings, K_xWO_3 plays a part in shielding most of NIR light and holding high Vis light transparency, while F-TiO_2 acts as both a photocatalyst to degrade harmful organic pollutants and a barrier to shield harmful ultraviolet light, which makes up the shortage of K_xWO_3 in the UV region. It's worth mentioning that the K_xWO_3 nanorods were synthesized with Na_2WO_4 as tungsten source instead of K_2WO_4, which is considered as a lower-cost way than previously reported method of preparing tungsten bronze powders[19,34]. Furthermore, the heat-shielding and photocatalytic property of F-TiO_2-K_xWO_3 nanocomposite films were evaluated and compared with that of ITO or P25 film to find out the optimal ratio of K_xWO_3 to F-TiO_2 with a synergistic effect.

Results and Discussion

As shown in Fig. 1, XRD analysis has been employed for analyzing the crystalline phase of samples. The reflection in Fig. 1a matches best with the single anatase TiO_2 (JCPDS 21-1272) phase, while the main peaks at 2θ values of 13.8°, 23.6° and 27.8° can be indexed respectively to (100), (002) and (200) crystal planes, which are readily indexed to the pure potassium tungsten bronze ($K_{0.26}WO_3$; JCPDS83-1593), as displayed in Fig. 1b. Furthermore, with the increasing content of F-TiO_2, the intensities of the TiO_2 peaks are increased obviously (Fig. 1c–g), revealing that FT-KWO nanocomposites are obtained successfully during the hydrothermal process. Meanwhile, peaks related to other phases are not observed in the synthesized samples, indicating that the F-TiO_2 have not reacted with the K_xWO_3.

The morphology of the as-prepared samples was characterized by SEM, which is shown in Fig. 2. As shown in Fig. 2a,b, the pure F-TiO_2 is nanoparticles with relatively uniform size and the as-prepared K_xWO_3 powders exhibit smooth surface, regular nanorods with size of about 300–400 nm, which are corresponding to that of products synthesized with K_2WO_4 and K_2SO_4[19]. Figure 2c shows the SEM image of K_xWO_3 samples after the introduction of the F-TiO_2, and it could be clearly seen that F-TiO_2 particles are attached to the surface of K_xWO_3 nanorods, indicating the intimate contact between F-TiO_2 and K_xWO_3. The inset in Fig. 2c shows the SEM image of FT/2KWO film at 45°, and the thickness of the film can be calculated to be about 3.37 μm, according to the equation: $t = t' \times \sin\theta$. Where t' is the thickness shown in SEM image ($t' = 2.38\,\mu m$) and θ is the view angle ($\theta = 45°$). In addition, EDX analysis confirms the distribution of Ti, O, F elements in F-TiO_2 samples and K, W, O elements in K_xWO_3 samples as shown in Fig. 2d,e, respectively. As for FT/2KWO nanocomposites (Fig. 2f), it reveals the coexistence of Ti, O, F, K, and W elements as expected, which also indicates the existence of F-TiO_2 and K_xWO_3 in FT/2KWO nanocomposites. Furthermore, according to EDX quantification (insert Fig. 2f), the atom percentages of Ti and W for the as-synthesized FT/2KWO nanocomposites are 9.74% and 6.62%, and the atom ratio of Ti to W is approximately 1.47, which is very close to the nominal value (Ti: W = 1.53). In addition,

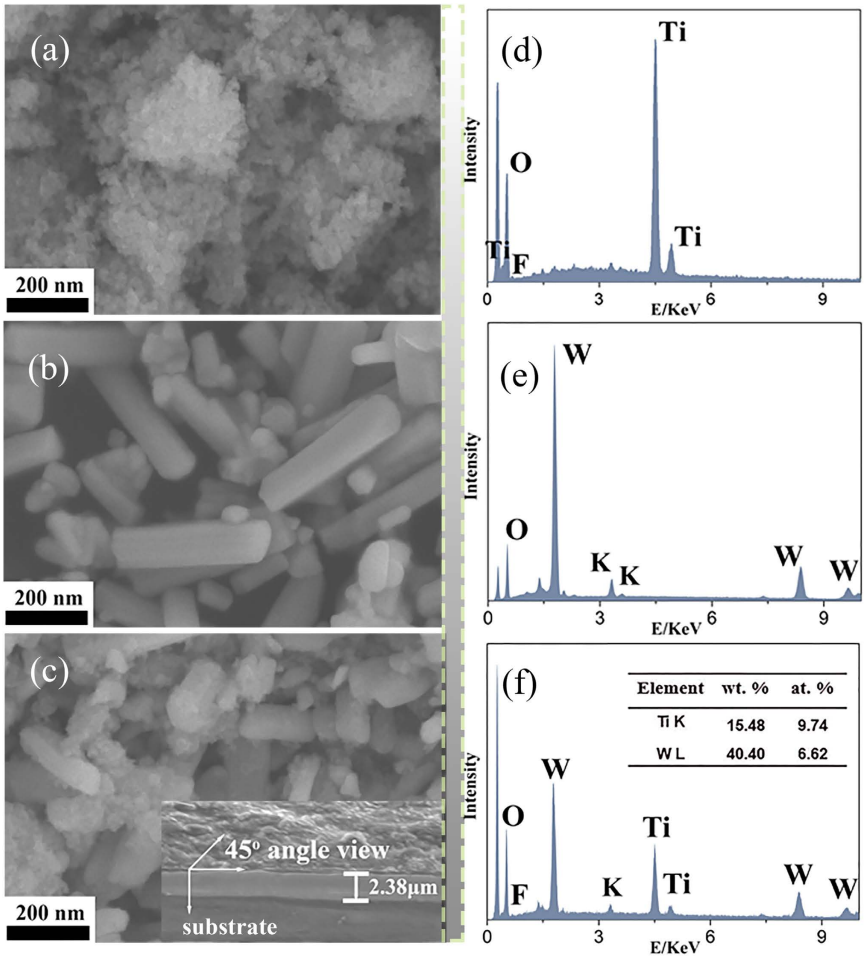

Figure 2. SEM images of (**a**) F-TiO_2, (**b**) K_xWO_3, (**c**) FT/2KWO nanocomposites; EDX spectra of (**d**) F-TiO_2, (**e**) K_xWO_3, (**f**) FT/2KWO nanocomposites. The insets in (**c**) shows SEM image of FT/2KWO films (at 45° angle view).

the Ti: W ratios are corresponding with the nominal ratios in all FT-KWO nanocomposites as displayed in Fig. S1, indicating that the elementary composition is well controlled by the experimental conditions.

To further obtain the microscopic morphology and structure information, the TEM and HRTEM analysis of as-synthesized FT/2KWO nanocomposites have been performed, as shown in Fig. 3. The TEM images of FT/2KWO nanocomposites (Fig. 3a,b) show the specific rod-like morphology with some nanoparticles attached, which is in accordance with SEM results. Moreover, The HRTEM image of the magnified view is given in Fig. 3c. The distance of 0.38 nm and 0.19 nm between the adjacent lattice fringes can be assigned to the (002) plane of hexagonal K_xWO_3 and the (200) plane of anatase TiO_2 nanocrystals, respectively. Obviously, the FT/2KWO nanocomposites are formed with favourable nanosizd interfacial contact so as to exhibit multifunctional properties of NIR shielding and photocatalytic degradation.

The chemical composition of the FT/2KWO nanocomposite particles was also examined by XPS. The full range XPS spectra are presented in Fig. S2a. Peaks at binding energies corresponding to Ti, O, F, K, and W are clearly distinguished and no extra elements except carbon can be found in the spectra. The W4f core-level XPS spectra of the as-prepared FT/2KWO samples exhibit detailed information on the chemical state of core level tungsten, as shown in Fig. S2b. There are two spin-orbit doublets in this spectrum, which is attributed to $W4f_{7/2}$ and $W4f_{5/2}$: the peaks at 35.8 eV and 37.9 eV are attributed to W^{6+}, while the peaks at 34.8 eV and 36.9 eV are assigned to W^{5+}, which reaches a good agreement with the reported results. Meanwhile, the atomic contents of Ti and W in FT/2KWO were calculated from XPS and found to be 55.23 at. % and 36.21 at. %, corresponding to the nominal value (Ti: W = 1.53). It is suggested that the non-stoichiometric potassium tungsten bronzes are reduced compounds, and the co-existence of W^{5+} and W^{6+} is the necessary condition for the NIR shielding performance[31].

To study optical properties of the samples, the transmittance spectra of the as-prepared films are shown in Fig. 4. For the pure K_xWO_3 film (Fig. 4g), a great NIR shielding performance at the range of 780 to 2500 nm was observed, which could be closely related to the plasmon resonance of free electrons, interband transition and small polarons[35]. However, the visible light transparency and absorption of ultraviolet region (see inset in Fig. 4) are defective. On the contrary, these phenomena above are absent in the case of the film of pure TiO_2 displayed in Fig. 4a, which exhibits no NIR shielding ability but excellent ultrviolet light absorption (see inset in Fig. 4) and high visible light transparency capability as a result of the narrow band gap of TiO_2. As expected, all of the

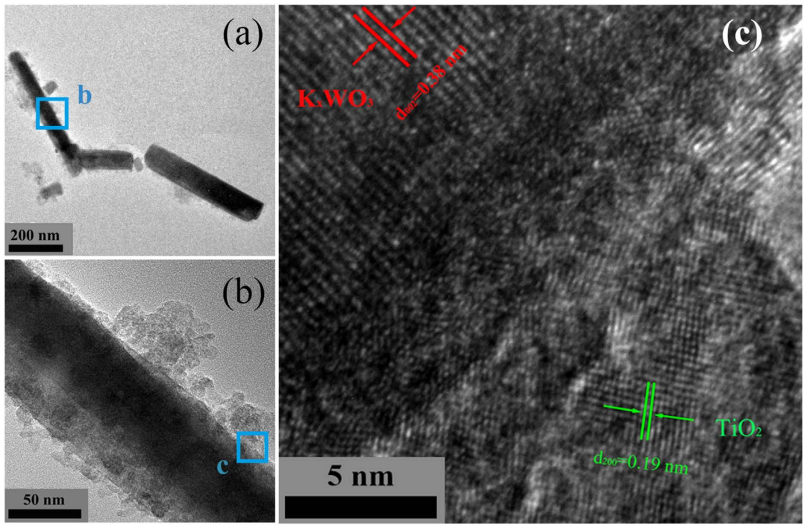

Figure 3. (**a**) Low-, (**b**) High-magnification TEM images and (**c**) HRTEM images of as-synthesized FT/2KWO nanocomposites.

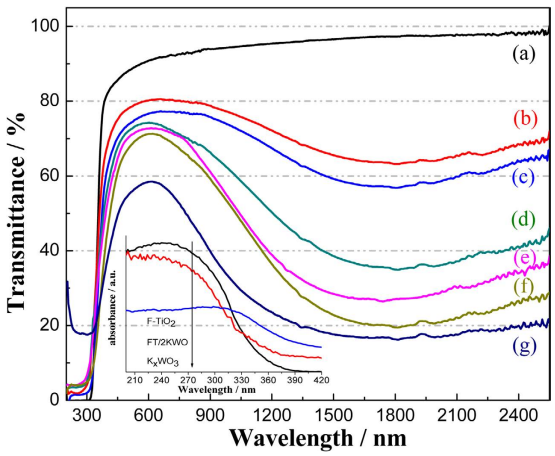

Figure 4. Transmittance spectra of (**a**) pure F-TiO_2, different FT-KWO nanocomposites: (**b**) 3FT/KWO, (**c**) 2FT/KWO, (**d**) FT/KWO, (**e**) FT/2KWO, (**f**) FT/3KWO and (**g**) pure K_xWO_3 films. The inset shows the absorption spectra of different powders with the wavelength from 200 nm to 420 nm.

FT-KWO nanocomposite films retain all advantages of TiO_2 and K_xWO_3 films in the range of UV, Vis and NIR. The inheritance of NIR absorption capability of composite could be attributed to the use of soft chemical method in synthesizing FT-KWO nanocomposite films in which the reduced W^{5+} ion was preserved. Specifically, with an increase in the K_xWO_3 content, the NIR shielding property becomes more pronounced while the visible light transmittance and UV shielding capability decreased. Even so, there will be a FT-KWO nanocomposite film with an appropriate mass ratio of F-TiO_2 to K_xWO_3, exhibiting a great synergistic effect on blocking NIR and UV light as well as transmitting most of visible light.

On the basis of the aforementioned optical properties of FT-KWO nanocomposite films, it is reasonable to suggest that these films show great potential for application as NIR shielding films. A thermal insulation experiment has been carried out in a sealed box. Figure 5 exhibits the inner temperature variation upon irradiation time and cooling time, and the temperature variations between the initial and final temperature are listed in Table S1. As shown in Fig. 5a, it's obvious that the temperature increases significantly with irradiation time when the box is covered with blank or F-TiO_2 coated glass, which proves that the F-TiO_2 film has no NIR shielding capacity as displayed in Fig. 4a. Notably, the heating rates of glasses coated with FT-KWO nanocomposites are much lower than those of box covered with the blank or F-TiO_2 coated glass, and the heating rate inside the box decreased distinctly with an increase in the K_xWO_3 content. For example, within 60 min irradiation, the temperature variation of box covered with 2FT/KWO nanoparticle film coated glass is 11.5 °C, while that of box covered with FT/2KWO film coated glass is depressed to 10.2 °C. In addition, the temperature variation curves with cooling time (Fig. 5b) show similar tendency as discussed above, that is to say, all of the FT-KWO nanocomposite films show good thermal insulation performance. Moreover, the temperature variation between the initial and final temperature slows

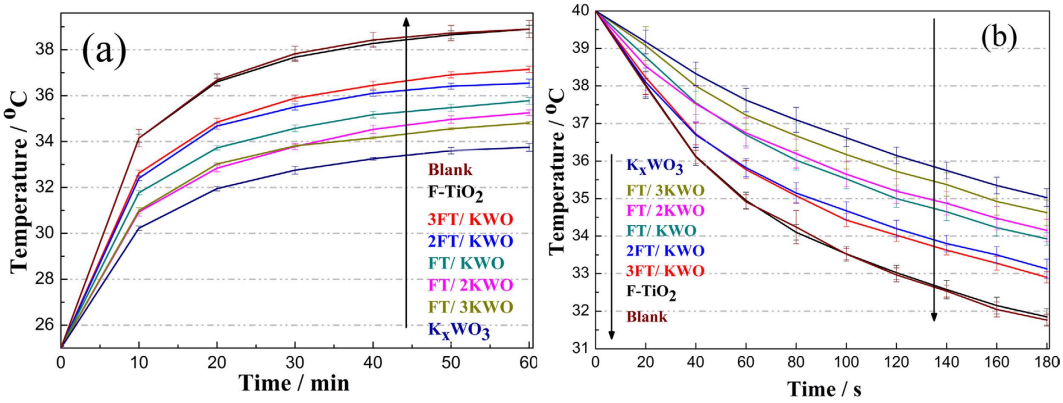

Figure 5. The inner temperature dependence on (**a**) irradiation time and (**b**) cooling time curves of sealed box covered with different films coated glass.

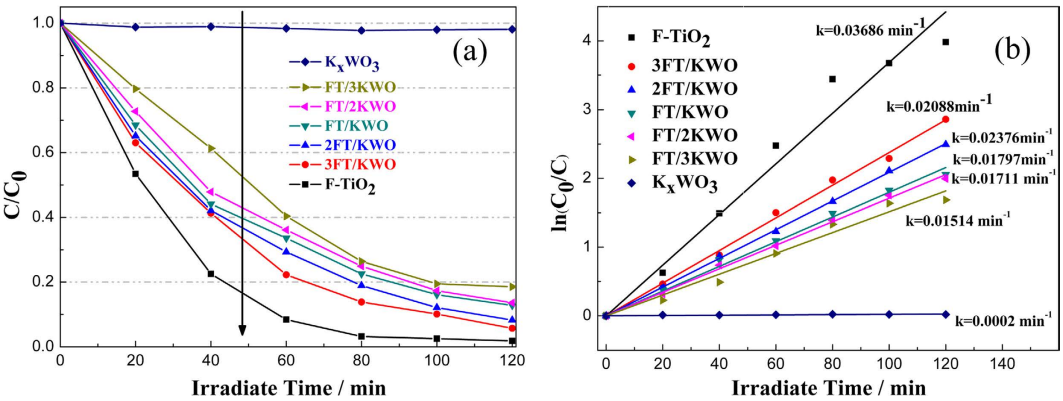

Figure 6. (**a**) Variation of MO concentration against irradiation time using F-TiO_2 film, FT-KWO nanocomposite films with various K_xWO_3 contents and pure K_xWO_3 film under ultraviolet light irradiation and (**b**) plots of ln (C_0/C) versus irradiation time for MO representing the fit using a pseudo-first-order reaction rate.

down with the increasing content of K_xWO_3, as displayed in Table S1. The relatively slow heating rates during the heating and cooling time indicate the FT-KWO nanocomposite films have great thermal insulation capacity. The ITO glasses are widely used and well-known as effective NIR shielding material, as a control, the simulated experiment was carried out by irradiating the sealed box covered by ITO, FT + 2KWO (mechanically mix F-TiO_2 and K_xWO_3), FT@2KWO (F-TiO_2 film coating on the top of K_xWO_3 film) and 2KWO@FT (K_xWO_3 film coating on the top of F-TiO_2 film) coated glass, respectively, and the temperature changes inside the boxes are plotted in Fig. S3a. By comparison, the box covered with the FT/2KWO film coated glass exhibited a slight lower temperature gradient than the box covered with other coated glasses both during the period of heating (Fig. S3a) and cooling (Fig. S3b). This phenomenon is corresponding to the transmittance spectra inserted in Fig. S3a. The results indicate superior thermal insulation capacity and potential practical application of the FT-KWO nanocomposite film.

In order to confirm the photocatalytic activities of FT-KWO nanocomposite films, the degradation of MO by various films was carried out under the irradiation of UV light. As shown in Fig. 6a, F-TiO_2 film exhibited high photocatalytic activity and 98% of the initial MO decreased after 80 min, whereas the K_xWO_3 film shows almost no effect on the degradation. Fortunately, these nanocomposite films are highly efficient for photocatalytic degradation of organic pollutant and the photocatalytic activity will be enhanced with the increase of F-TiO_2 content in FT-KWO nanocomposites. For example, about 87% of the initial MO molecules are decomposed by the 3FT/KWO nanocomposite film, while in comparison, only 73% by the FT/3KWO film within 80 min. Based on previous studies, the degradation of dyes can be ascribed to a pseudo-first order reaction with a Langmuir–Hinshelwood model when the initial concentration of dye solution is small: $\ln(C_0/C) = kt$[36]. Where C is the concentration of MO after t min degradation, C_0 is the initial concentration of MO, and k is the first-order reaction rate constant. Figure 6b exhibits the plots of ln (C_0/C) versus irradiation time. Unusually, the FT/2KWO film exhibits similar photocatalytic activity to FT/KWO film where the k of FT/KWO is only about 1.05 times than that of FT/2KWO. Meanwhile, considering the temperature variation curves displayed in Fig. 5, the thermal insulation capacity of FT/2KWO film has gained a noticeable improvement than that of FT/KWO film. In other words, the FT-KWO film shows the best multifunctional properties when the mass ratio of F-TiO_2 to K_xWO_3 is 1:2. To further investigate the advantages of FT-KWO nanocomposite film, as a comparison, the photocatalytic activities of P25, FT + 2KWO, FT@2KWO, 2KWO@FT and F-TiO_2' (where the F-TiO_2 content in this film is equal to that of FT/2KWO film) films were measured under the same condition. As displayed in Fig. S4, the photocatalytic

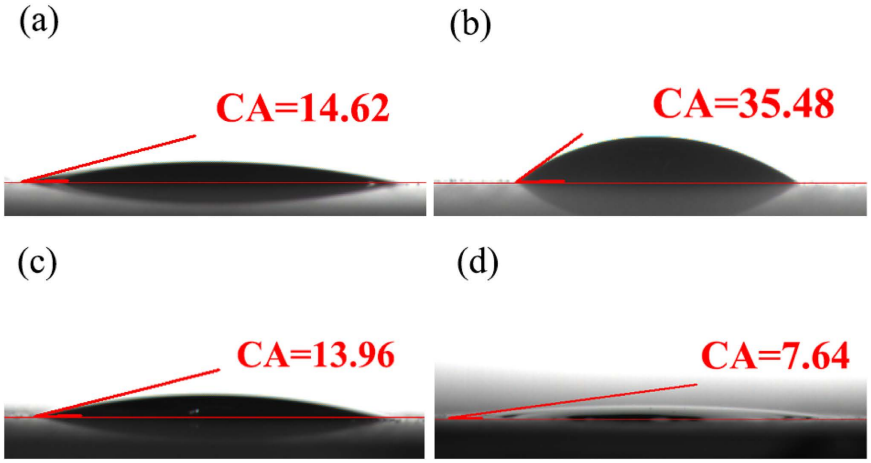

Figure 7. Contact angle of a water drop in air on new (**a**) F-TiO_2, (**b**) K_xWO_3, (**c**) FT/2KWO films and (**d**) FT/2KWO film after the fourth photocatalytic experiment.

activity sequence of these films is FT/2KWO ~ P25 > FT + 2KWO > F-TiO_2' ~ FT@2KWO > 2KWO@FT and the enhancement of the photocatalytic activity could be attributed to the close interfacial contact and strong interaction between F-TiO_2 and K_xWO_3 in FT/2KWO film. Besides, the introduction of K_xWO_3 with excellent electronic conductivity can promote the photogenerated electron transport to the surface of the composite more easily, thus inhibiting the recombination between photogenerated electrons and holes[34,37,38]. However, when it comes to FT + 2KWO film and others, the F-TiO_2 and K_xWO_3 are independent (see SEM image inset Fig. S4) to generate nearly no synergistic effect. It is abnormal that only 53% of the initial MO molecules are decomposed by 2KWO@FT nanocomposite film within 120 min, which might be attributed to the covered surface of F-TiO_2 limits the photocatalytic reaction to some extent[39]. In conclusion, these results mentioned above further confirm that the FT/2KWO nanocomposite film is effective for photocatalytic degradation of organic pollutant and very promising for practical application in smart window.

In consideration of the practical application of these nanocomposite films, the photocatalytic stability of the as-prepared FT/2KWO nanocomposite film was further investigated by the cycle experiment. As shown in Fig. S5a, the photocatalytic activity of the FT/2KWO nanocomposite film remains still unreduced after four consecutive cycles, thus indicating the good stability of the film during the photocatalytic experiment. Furthermore, the thermal insulation capacity of the FT/2KWO film after the fourth photocatalytic experiment was investigated and exhibited in Fig. S5b. It is clear that the temperature variation of box is about 10.5 °C (Fig. S5b-2) when it was covered with the FT/2KWO film coated glass after the fourth photocatalytic experiment, which is slightly higher than that of new FT/2KWO film coated glass (Fig. S5b-3), but much lower than that of blank glass (Fig. S5b-1). It thus indicates the great reusability of the FT-KWO nanocomposite films.

To identify the surface hydrophilic properties of the nanocomposite films, the contact angle (CA) value of the as-prepared FT/2KWO film was measured and compared with that of pure TiO_2, K_xWO_3 film, as shown in Fig. 7. Notably, the CA value of K_xWO_3 film (CA = 35.48) is significantly higher than that of F-TiO_2 film (CA = 14.62), which indicates the F-TiO_2 film has good hydrophilic property. Meanwhile, the CA value of FT/2KWO film (CA = 13.96) has not been affected by the introduction of K_xWO_3 and the similar CA values between F-TiO_2 film and FT/2KWO film reveal the hydrophilic nature of prepared FT/2KWO film. Interestingly, the CA value of FT/2KWO film decreased to 7.64° after the fourth photocatalytic experiment, as displayed in Fig. 7d. This phenomenon could be attributed to the photoinduced hydrophilicity caused by reconstruction of surface hydroxyl groups[40,41]. The above results confirm the FT/2KWO film is advantageous for applications in antifogging and self-cleaning coatings.

A working model illustrating the multifunctionality of the FT-KWO and F-TiO_2 coated window is summarized in Fig. 8. Obviously, this smart window plays different roles in various conditions. In summer days, the FT-KWO film side towards the outside; with the irradiation of the solar light, the smart window can not only block most of the NIR lights for heat preservation and keep cool indoor, but also isolate harmful UV light and transmit Vis light. In winter days, this window should be rotated 180° to make the FT-KWO film side towards the inside. In this case, the smart window not only reduces heat loss from inside to outside, but also blocks UV light and transmits Vis light effectively. Meanwhile, the high hydrophilic capacity can control the production of water vapour on the window and enhance the visibility availably. To sum up, this smart window will minimize the usage of air conditioning and heaters to control the redundant electricity consumption and promote the solution of energy crisis. In addition, both sides will absorb UV light to motivate photocatalytic reaction owing to the existence of F-TiO_2, so as to degrade the harmful organic air pollutants and help solve the environmental issues subtly.

In summary, the F-TiO_2-K_xWO_3 multifunctional nanocomposites have been fabricated successfully through a low-cost and eco-friendly method. Moreover, the FT-KWO films exhibited excellent multifunctional performance of NIR, UV light insulation, Vis transparency and photocatalytic activity. A competitive relation was observed between F-TiO_2 and K_xWO_3: the photocatalytic activity will be decreased while the thermal insulation

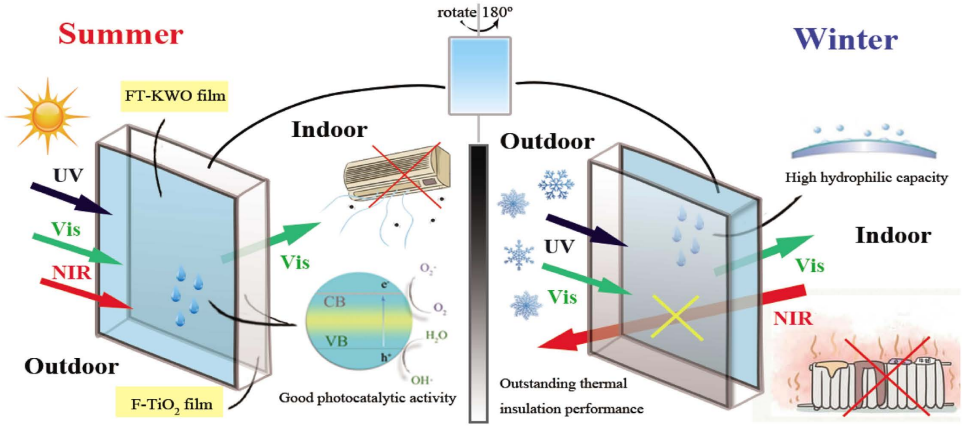

Figure 8. The working model of the FT-KWO and F-TiO_2 coated window applied to different conditions.

performance improved with the increase of K_xWO_3 content in FT-KWO nanocomposite films. As the optimal proportion of K_xWO_3 to F-TiO_2, the FT/2KWO nanocomposite film shows a significant multifunctional property of outstanding NIR, UV light shielding performance, high photocatalytic activity on degradation of harmful organic pollutants and excellent hydrophilic capacity. It is worth mentioning that its thermal insulation capacity is better than that of ITO, while the photocatalytic activity is surpassing P25. Therefore, FT-KWO nanocomposite film could have great potential applications as smart windows coating material, so as to help solve the energy crisis and deteriorating environmental issues in a convenient way.

Methods

Preparation of K_xWO_3 nanorods. K_xWO_3 nanorods were synthesized on the basis of a procedure reported previously. All reagents were of analytical grade and used without further retreatment. Specifically, 1.6493 g $Na_2WO_4{\cdot}2H_2O$ and 1.7424g K_2SO_4 were dissolved in 50 ml deionized water under magnetic stirring followed by adding 3 mol/L HCl to adjust pH to 1.5. After that, the resultant solution was transferred into a dried Teflon-lined autoclave with 100 mL internal volume and kept it at 200 °C for 24 h. After natural cooling to room temperature, the intermediate products were obtained after being washed with water and ethanol for three times respectively and dried at 50 °C overnight. Finally, a certain amount of as-prepared samples was reduced in H_2 (5 vol %)/N_2 atmosphere at 500 °C for 1 h to obtain the potassium tungsten bronze.

Preparation of FT-KWO nanocomposites. The as-prepared K_xWO_3 nanorods were redispersed via the assist of ultrasonication in 30 mL deionized water to obtain the homogeneous suspension. Then, 0.0713g NH_4HF_2 and 7.5 ml absolute ethyl alcohol with 1.71 ml tetrabutyl titanate (TBOT) were added dropwise to the suspensions under vigorous stirring for 30 min. Finally, the above suspensions were transferred into 50 mL Teflon-lined autoclaves and maintained at 150 °C for 10 h. After this hydrothermal reaction, the suspensions were centrifuged at 17000 rpm followed by washing with distilled water and ethanol twice, and then dried in an oven at 80 °C for 2 h. The nominal contents of K_xWO_3 additives were 25 wt.%, 33 wt.%, 50 wt.%, 67 wt.% and 75 wt.%, respectively for the FT-KWO nanocomposites. These samples are labelled as 3FT (F-TiO_2)/KWO (K_xWO_3), 2FT/KWO, FT/KWO, FT/2KWO, and FT/3KWO, respectively. For comparison, pure F-TiO_2 and K_xWO_3 were synthesized under the same condition.

Preparation of FT-KWO nanocomposite films. The NIR shielding and photocatalysis properties of F-TiO_2-K_xWO_3 nanocomposites were evaluated by coating them onto quartz glass substrates (4 cm*4 cm*1 mm). In a typical film synthesis process, 0.2 g samples were dispersed into a mixed solution with 1.24 g collodion and 1.33 g absolute ethyl alcohol under magnetically stirring, thus forming homogeneous colloidal dispersions. Subsequently, the above slurries were spin-coated on the quartz glass substrates at 2500 rpm for 60 s, rinsed with absolute ethyl alcohol and dried at 60 °C for 30 min. For comparison, the P25, ITO and blank films were prepared under the identical conditions. In addition, the synthesis process of other films was presented in the supporting information.

Characterization. The phase purity of samples was analyzed by X-ray powder diffraction (XRD) using a Bruker D2 PHASER X-ray diffractometer with graphite monochromator using Cu Kα radiation ($\lambda = 1.54184$ Å) at room temperature. The morphology of the sample and the energy dispersive X-ray spectroscopy (EDS) spectrum were detected by field emission scanning electron microscopy (FESEM, Hitachi, 30 S-4800). Moreover, the transmittance of films was measured with a Perkin Elmer 950 spectrometer. Besides, transmission electron microscopy (TEM) and high-resolution transmission electron microscopy (HRTEM) images were collected on an F30 S-TWIN electron microscope (Tecnai G2, FEI Company). X-ray photoelectron spectroscopy (XPS, PHI-5702, Physical Electronics) was performed using a monochromated Al Ka irradiation. The chamber pressure was ~3×10^{-8} Torr under testing conditions. The surface hydrophilic properties of the as-prepared films were

characterized by detecting the water contact angle measured by a contact angle meter (JC2000C) with 4 μL water droplet under ambient conditions.

Evaluation of NIR shielding property. To evaluate the thermal insulation properties of FT-KWO nanocomposite films, a simulated room was built with a sealed plastic box (11 cm*11 cm*11 cm) covered with different films coated glasses under the irradiation of a 275 W infrared lamp. The experiments were carried out at the room temperature of 25 °C and temperature variation was monitored by a thermodetector with four thermocouples every ten minutes. Meanwhile, the heat preservation performance of these films was evaluated in the same plastic box without the irradiation of infrared lamp, but the glasses were rotated 180° to make the FT-KWO film side toward the inside with the initial temperature being 40 °C.

Evaluation of photocatalytic activity. The photocatalytic activities of the FT-KWO nanocomposite films were evaluated by measuring the degradation ratio of methyl orange (MO). The initial concentration of MO solution was 10 mg/L^{-1}, and the quartz glass substrate coated with FT-KWO nanocomposite film was immersed in 5 mL MO solution. A 500 W high pressure Hg lamp was employed for the ultraviolet irradiation source and positioned 10 cm away from the reactor to trigger the photocatalytic reaction. In addition, a certain volume of MO solution was withdrawn at selected times and analysed by measuring the light absorption of the clear solution at 464 nm (λ_{max} for MO solution) using a spectrophotometer (LG-722SP).

References

1. Ong, W.-J., Tan, L.-L., Chai, S.-P., Yong, S.-T. & Mohamed, A. R. Facet-Dependent Photocatalytic Properties of TiO_2-Based Composites for Energy Conversion and Environmental Remediation. *Chem Sus Chem* **7,** 690–719 (2014).
2. Yue, D., You, F. & Darling, S. B. Domestic and overseas manufacturing scenarios of silicon-based photovoltaics: Life cycle energy and environmental comparative analysis. *Solar Energy* **105,** 669–678 (2014).
3. Wang, W. *et al.* Monoclinic dibismuth tetraoxide: A new visible-light-driven photocatalyst for environmental remediation. *Applied Catalysis B: Environmental* **176–177,** 444–453 (2015).
4. Wen, C., Cui, Y., Chen, X., Zong, B. & Dai, W.-L. Reaction temperature controlled selective hydrogenation of dimethyl oxalate to methyl glycolate and ethylene glycol over copper-hydroxyapatite catalysts. *Applied Catalysis B: Environmental* **162,** 483–493 (2015).
5. Qureshi, M. I., Rasli, A. M. & Zaman, K. Energy crisis, greenhouse gas emissions and sectoral growth reforms: repairing the fabricated mosaic. *Journal of Cleaner Production* **112,** Part 5, 3657–3666 (2016).
6. Guo, C., Yin, S., Dong, Q. & Sato, T. Simple route to $(NH_4)_{(x)}WO_3$ nanorods for near infrared absorption. *Nanoscale* **4,** 3394–8 (2012).
7. Guo, C., Yin, S., Sato, T. & Priya, S. Effects of Crystallization Atmospheres on the Near-Infrared Absorbtion and Electroconductive Properties of Tungsten Bronze Type M_xWO_3 (M = Na, K). *Journal of the American Ceramic Society* **95,** 1634–1639 (2012).
8. Kreibig, U. & Vollmer., M. Optical properties of metal clusters. *Springer Ser. Mat. Sci* **25** (1995).
9. Takeda H., Otsuka Y., Kuno H. & Adachi K. Inventors; Sumitomo Metal Mining Company, Limited, assignee. Coating solution for a heat-ray shielding film and a process for forming a heat-ray shielding film by employing the same. United States patent US 5,840,364. 1998 Nov 24.
10. Adachi, K., Miratsu, M. & Asahi, T. Absorption and scattering of near-infrared light by dispersed lanthanum hexaboride nanoparticles for solar control filters. *Journal of Materials Research* **25,** 510–521 (2010).
11. Takeda, H. & Adachi, K. Near Infrared Absorption of Tungsten Oxide Nanoparticle Dispersions. *Journal of the American Ceramic Society* **90,** 4059–4061 (2007).
12. Feng, J., Huang, B. & Zhong, M. Fabrication of superhydrophobic and heat-insulating antimony doped tin oxide/polyurethane films by cast replica micromolding. *Journal of Colloid and Interface Science* **336,** 268–272 (2009).
13. Okuhara, Y., Kato, T., Matsubara, H., Isu, N. & Takata, M. Near-infrared reflection from periodically aluminium-doped zinc oxide thin films. *Thin Solid Films* **519,** 2280–2286 (2011).
14. Liu, H., Zeng, X., Kong, X., Bian, S. & Chen, J. A simple two-step method to fabricate highly transparent ITO/polymer nanocomposite films. *Applied Surface Science* **258,** 8564–8569 (2012).
15. Luther, J. M., Jain, P. K., Ewers, T. & Alivisatos, A. P. Localized surface plasmon resonances arising from free carriers in doped quantum dots. *Nat Mater* **10,** 361–6 (2011).
16. Guo, C. *et al.* Novel synthesis of homogenous Cs_xWO_3 nanorods with excellent NIR shielding properties by a water controlled-release solvothermal process. *Journal of Materials Chemistry* **20,** 8227 (2010).
17. Guo, C. *et al.* Photothermal ablation cancer therapy using homogeneous Cs_xWO_3 nanorods with broad near-infra-red absorption. *Nanoscale* **5,** 6469–78 (2013).
18. Shi, F. *et al.* Hydrothermal Synthesis of Cs_xWO_3 and the Effects of N_2 Annealing on its Microstructure and Heat Shielding Properties. *Journal of Materials Science & Technology* **30,** 342–346 (2014).
19. Guo, C., Yin, S., Huang, L. & Sato, T. Synthesis of one-dimensional potassium tungsten bronze with excellent near-infrared absorption property. *ACS Appl Mater Interfaces* **3,** 2794–9 (2011).
20. Yu, X. *et al.* Cu_2ZnSnS_4-Pt and Cu_2ZnSnS_4-Au Heterostructured Nanoparticles for Photocatalytic Water Splitting and Pollutant Degradation. *Journal of the American Chemical Society* **136,** 9236–9239 (2014).
21. Jang, E. S., Won, J. H., Hwang, S. J. & Choy, J. H. Fine Tuning of the Face Orientation of ZnO Crystals to Optimize Their Photocatalytic Activity. *Advanced Materials* **18,** 3309–3312 (2006).
22. Quintana, M., Edvinsson, T., Hagfeldt, A. & Boschloo, G. Comparison of Dye-Sensitized ZnO and TiO_2 Solar Cells: Studies of Charge Transport and Carrier Lifetime. *The Journal of Physical Chemistry C* **111,** 1035–1041 (2007).
23. Morimoto, T., Tomonaga, H. & Mitani, A. Ultraviolet ray absorbing coatings on glass for automobiles. *Thin Solid Films* **351,** 61–65 (1999).
24. Savio, A. K. P. D. *et al.* Environmentally effective photocatalyst CoO–TiO_2 synthesized by thermal precipitation of Co in amorphous TiO_2. *Applied Catalysis B: Environmental* **182,** 449–455 (2016).
25. Jaiswal, R. *et al.* Efficient Co-B-codoped TiO_2 photocatalyst for degradation of organic water pollutant under visible light. *Applied Catalysis B: Environmental* **183,** 242–253 (2016).
26. Han, C., Yang, M. Q., Weng, B. & Xu, Y. J. Improving the photocatalytic activity and anti-photocorrosion of semiconductor ZnO by coupling with versatile carbon. *Phys Chem Chem Phys* **16,** 16891–903 (2014).
27. Mutin, P. H. *et al.* Selective Surface Modification of SiO_2-TiO_2 Supports with Phosphonic Acids. *Chemistry of Materials* **16,** 5670–5675 (2004).
28. Wang, Q., Chen, C., Zhao, D., Ma, W. & Zhao, J. Change of Adsorption Modes of Dyes on Fluorinated TiO_2 and Its Effect on Photocatalytic Degradation of Dyes under Visible Irradiation. *Langmuir* **24,** 7338–7345 (2008).
29. Park, J. S. & Choi, W. Enhanced Remote Photocatalytic Oxidation on Surface-Fluorinated TiO_2. *Langmuir* **20,** 11523–11527 (2004).

30. Yu, J., Wang, W., Cheng, B. & Su, B.-L. Enhancement of Photocatalytic Activity of Mesporous TiO_2 Powders by Hydrothermal Surface Fluorination Treatment. *The Journal of Physical Chemistry C* **113,** 6743–6750 (2009).
31. Wu, X., Yin, S., Xue, D., Komarneni, S. & Sato, T. A Cs_xWO_3/ZnO nanocomposite as a smart coating for photocatalytic environmental cleanup and heat insulation. *Nanoscale* **7,** 17048–17054 (2015).
32. Wang, Y., Shi, R., Lin, J. & Zhu, Y. Enhancement of photocurrent and photocatalytic activity of ZnO hybridized with graphite-like C_3N_4. *Energy & Environmental Science* **4,** 2922–2929 (2011).
33. Huang, T. H. *et al.* Resistive memory for harsh electronics: immunity to surface effect and high corrosion resistance via surface modification. *Sci Rep* **4,** 4402 (2014).
34. Liu, B. *et al.* Graphene/M_xWO_3 (M = Na, K) nanohybrids with excellent electrical properties. *Carbon* **94,** 309–316 (2015).
35. Guo, C., Yin, S., Huang, L., Yang, L. & Sato, T. Discovery of an excellent IR absorbent with a broad working waveband: $Cs_{(x)}WO_3$ nanorods. *Chem Commun* (*Camb*) **47,** 8853–5 (2011).
36. Sakkas, V. A. *et al.* Metolachlor photocatalytic degradation using TiO_2 photocatalysts. *Applied Catalysis B: Environmental* **49,** 195–205 (2004).
37. Liu, B. *et al.* A Facile One-Step Solvothermal Synthesis and Electrical Properties of Reduced Graphene Oxide/Rod-Shaped Potassium Tungsten Bronze Nanocomposite. *Journal of Nanoscience and Nanotechnology* **15,** 7305–7310 (2015).
38. Yu, H., Tian, J., Chen, F., Wang, P. & Wang, X. Synergistic Effect of Dual Electron-Cocatalysts for Enhanced Photocatalytic Activity: rGO as Electron-Transfer Mediator and Fe(III) as Oxygen-Reduction Active Site. *Sci Rep* **5,** 13083 (2015).
39. Tang, J., Quan, H. & Ye, J. Photocatalytic Properties and Photoinduced Hydrophilicity of Surface-Fluorinated TiO_2. *Chemistry of Materials* **19,** 116–122 (2007).
40. Sakai, N., Fujishima, A., Watanabe, T. & Hashimoto, K. Quantitative Evaluation of the Photoinduced Hydrophilic Conversion Properties of TiO_2 Thin Film Surfaces by the Reciprocal of Contact Angle. *The Journal of Physical Chemistry B* **107,** 1028–1035 (2003).
41. Sakai, N., Fujishima, A., Watanabe, T. & Hashimoto, K. Enhancement of the Photoinduced Hydrophilic Conversion Rate of TiO_2 Film Electrode Surfaces by Anodic Polarization. *The Journal of Physical Chemistry B* **105,** 3023–3026 (2001).

Acknowledgements

This research was supported by the International Sci. & Tech. Cooperation Foundation of Gansu Provincial, China (Grant Nos 1504WKCA088 and 1304WCGA177), the National Science Foundation for Fostering Talents in Basic Research of National Natural Science Foundation of China (Nos 041105 and 041106), the National Natural Science Funds of China (Grant No. 51372105) and the Network Joint Research Center for Materials and Devices, the Grant-in-Aid for Science Research (No. 23241025).

Author Contributions

T.L. and B.L. conducted the most of investigation for the samples. T.L. wrote the main paper. B.L. designed the concept and the experiment method of the research. B.L. and Y.W. supervised the project, had given valuable advices on the proceeding of this work and revised the manuscript. S.Y., T.S. and T.S. had provided precious suggestions on the selection of tungsten bronze as NIR shielding materials. J.W., Y.Z. and L.Y. supported the characterization of the samples. H.L. and X.M. revised the manuscript. All authors discussed the results and commented on the manuscript at all stages.

Additional Information

Supplementary information accompanies this paper at http://www.nature.com/srep

Competing financial interests: The authors declare no competing financial interests.

How to cite this article: Liu, T. *et al.* Smart window coating based on F-TiO_2-K_xWO_3 nanocomposites with heat shielding, ultraviolet isolating, hydrophilic and photocatalytic performance. *Sci. Rep.* **6**, 27373; doi: 10.1038/srep27373 (2016).